Fast Beamforming of Electronically Steerable Parasitic Array Radiator Antennas: Theory and Experiment

Chen Sun, *Student Member, IEEE*, Akifumi Hirata, *Member, IEEE*, Takashi Ohira, *Fellow, IEEE*, and Nemai C. Karmakar, *Senior Member, IEEE*

***Abstract*—A low-power consumption, small-size smart antenna, named electronically steerable parasitic array radiator (ESPAR), has been designed. Beamforming is achieved by tuning the load reactances at parasitic elements surrounding the active central element. A fast beamforming algorithm based on simultaneous perturbation stochastic approximation with a maximum cross correlation coefficient criterion is proposed. The simulation and experimental results validate the algorithm. In an environment where the signal-to-interference-ratio is 0 dB, the algorithm converges within 50 iterations and achieves an output signal-to-interference-plus-noise-ratio of 10 dB. With the fast beamforming ability and its low-power consumption attribute, the ESPAR antenna makes the mass deployment of smart antenna technologies practical.**

***Index Terms*—Ad hoc network, aerial beamforming (ABF), digital beamforming (DBF), electronically steerable parasitic array radiator (ESPAR), simultaneous perturbation stochastic approximation (SPSA), smart antennas, spatial division multiple access (SDMA).**

I. Introduction

THE EXPLOSIVE growth of wireless communications industry is creating a huge market opportunity. Wireless operators are currently searching for new technologies which would be implemented into the existing wireless communications infrastructures to provide the broader bandwidth per user channel, the better quality and new value-added services. Smart antennas or adaptive arrays have gained great interest among researchers. Deployed at the base station of the existing wireless infrastructures, it brings an outstanding capacity improvement to the frequency resource limited radio communications system by an efficient frequency reuse scheme. New value added services, such as the position location (PL) services for an emergency call, the fraud detection, the intelligent transportation system etc., are also coming into reality with the direction finding ability of smart antennas [1], [2]. It also has the applications in ad hoc networks or wireless local-area networks (WLANs), for example employed at mobile terminals (notebooks, PDAs, etc.) in a wireless network. The direction finding ability avails the design of the packet routing protocol, which decides the manner of packet relaying. The beamforming or interference suppression ability makes it possible to increase the throughput at the network nodes that is limited by interferences from neighboring nodes [3].

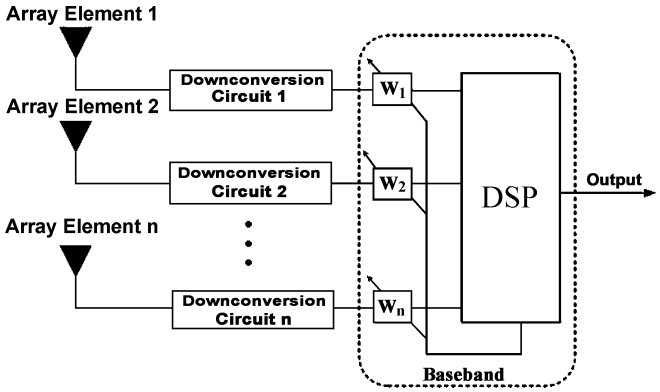

Fig. 1. Functional block diagram of DBF antenna arrays using phased array technology.

Various beamforming and direction-of-arrival (DOA) estimation algorithms have been designed [4]. The simulation and experiments carried out by many researchers have shown the abilities of these algorithms. Most of these algorithms are designed based on the digital beamforming (DBF) antenna arrays (see Fig. 1). Signals received by individual antenna elements are down-converted into baseband signals. These signals are digitized and fed into digital signal processing (DSP) chip where the algorithms reside in. However, RF circuit branches connected to the array elements, analog-to-digital converters (ADCs) and the baseband DSP chip consume a considerable amount of dc power. Furthermore, each channel connected to the array sensor has the same structure, so the cost of fabrication increases with the number of array elements [5]. Thanks to the recent development of GaAs monolithic microwave integrated circuit (MMIC) technologies, the beamformer could be integrated into a single chip at the RF front end [microwave beamforming (MBF)] [6], instead of the baseband. The advantages are the reduced quantization errors and the increased dynamic range. However, their costs of fabrication still limit

Manuscript received April 30, 2003; revised August 6, 2003. The work was supported in part by the Telecommunications Advancement Organization of Japan.

C. Sun was with the Advanced Telecommunications Research Institute International (ATR), 619-0288 Kyoto, Japan. He is now with the School of Electrical and Electronic Engineering, Nanyang Technological University, 639-798 Singapore, Singpaore (e-mail: csun@ieee.org).

A. Hirata and T. Ohira are with the Adaptive Communications Research Laboratories, Advanced Telecommunications Research Institute International (ATR), 619-0288 Kyoto, Japan.

N. C. Karmakar is with the School of Electrical and Electronic Engineering, Nanyang Technological University, 639-798 Singapore, Singapore.

Digital Object Identifier 10.1109/TAP.2004.831314

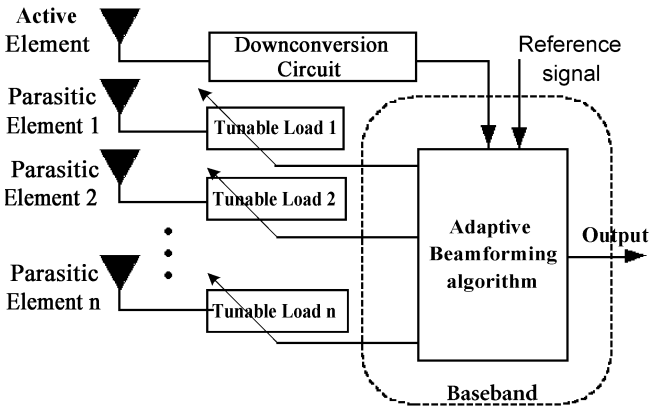

Fig. 2. Functional block diagram of ESPAR antennas.

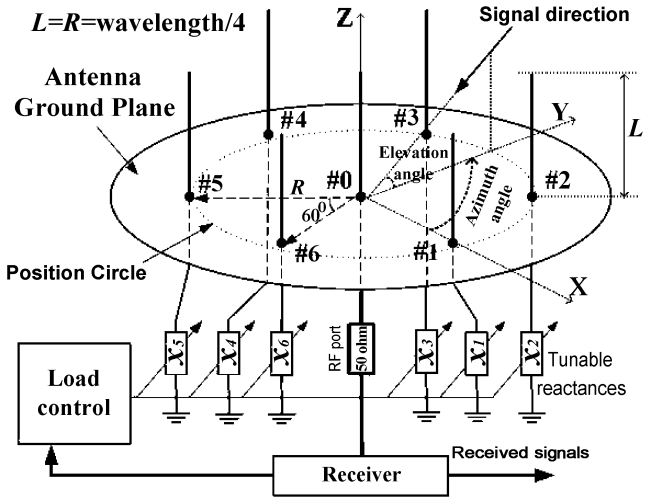

Fig. 3. Configuration of a seven-element ESPAR antenna. The length of each monopole L and the radius R of the circular grid are one-quarter wavelength of the transmitting RF signal at 2.484 GHz.

the range of implementations. All these factors make DBF and MBF antennas unsuitable for low-power consumption and low cost systems and hinder the mass applications of the smart antenna technologies. For example, it could be too costly to equip DBF antenna arrays at battery powered lap-tops or mobile computing terminals within a wireless network.

ESPAR antennas can circumvent the DBF and MBF deployment problems. It is a reactively controlled directive array antenna [7], [8], in which one central element connected to the sole RF port and a number of surrounding parasitic elements form the array. Beam steering is achieved by tuning the load reactances at parasitic elements surrounding the central active element (see Fig. 2). The load reactances are realized by the reversely biased (RB) varactor diodes. There is only a small RB leakage current. Therefore, the power consumption of the ESPAR antenna is very small. Furthermore, the system has only one RF port and one consequent down-conversion circuit. From the viewpoints of the power consumption and the fabrication cost, it is obvious that the ESPAR antennas are suitable for mass implementations of smart antennas, especially for battery powered portable mobile terminals.

As aforementioned, the direction finding and the adaptive beamforming are two important issues of smart antenna technologies. The DOA estimation with a modified multiple signal classification (MUSIC) algorithm has been successfully realized for ESPAR antennas [9]–[14]. But the reported beamforming algorithms [15]–[20] are still not efficient enough for real time implementations in the wireless communications systems, where a fast beam tuning ability is required. In this paper a fast beamforming algorithm based on the SPSA is proposed. After the theoretical study and the simulation the performance is examined with experiments at a radio anechoic chamber. The excellent agreement between the simulation and the experimental results reflects the effectiveness of the proposed beamforming algorithm. Our study proves the adaptive beamforming ability of the ESPAR antennas and demonstrates its suitability for mass commercial implementations of smart antenna technologies to wireless networks.

The paper is organized as follows: Section II presents the configuration and the working principle of the ESPAR antenna. The proposed beamforming algorithm is presented in Section III. Section IV gives the simulation results and discussions. The antenna testbed and experimental results are described in Section V and VI followed by the discussion and conclusions in Section VII.

II. Theory of ESPAR Antennas

A. Configuration and Working Principle

Fig. 3 shows the configuration of a seven-element ESPAR antenna. One active central element (monopole) is surrounded by six parasitic elements uniformly placed on a circular grid of radius R on a circular grounded baseplate. The length of each monopole L and the radius R of the circular grid are one-quarter wavelength $(\lambda/4)$ of the transmitting RF signal at 2.484 GHz. According to Harrington [7], large spacing among elements (for example $\lambda/2$) leads to reduced gain and significant back lobes. And further reduce to $\lambda/8$ leads to the super-gain array. Therefore, a realistic design for spacing $= \lambda/4$ is chosen. The baseplate transforms monopoles with their images to dipoles with a length of $2L$. The central monopole is connected to a RF receiver and each parasitic monopole is loaded with a tunable varactor.

The working principle of ESPAR antennas is different from that for DBF array antennas. We first assume that the antenna is working in the transmitting mode. The antenna generates a directional beam based on tuning load reactances $(x_1, x_2, \ldots, x_6)$ on the parasitic monopoles. Signals received or transmitted from the central RF port excite the parasitic monopoles with substantial induced mutual currents on them. Vectors I and V represent the currents and the voltages on the monopoles, respectively

$$I = [i_0 \quad i_1 \quad i_2 \quad i_3 \quad i_4 \quad i_5 \quad i_6]^T \tag{1}$$

$$V = [v_0 \quad v_1 \quad v_2 \quad v_3 \quad v_4 \quad v_5 \quad v_6]^T. \tag{2}$$

The superscript T represents the transpose. i_0 and v_0 represent the current and the voltage on the active central element (♯0), respectively. Mutual admittances are represented by the matrix $\mathbf{Y}$ with each entity y_{ij} denoting the mutual admittance between

the ith element and the jth element. The induced currents are represented with mutual admittances

$$I = \mathbf{Y}V = \begin{bmatrix} y_{00} & y_{01} & y_{02} & y_{03} & y_{04} & y_{05} & y_{06} \\ y_{10} & y_{11} & y_{12} & y_{13} & y_{14} & y_{15} & y_{16} \\ y_{20} & y_{21} & y_{22} & y_{23} & y_{24} & y_{25} & y_{26} \\ y_{30} & y_{31} & y_{32} & y_{33} & y_{34} & y_{35} & y_{36} \\ y_{40} & y_{41} & y_{42} & y_{43} & y_{44} & y_{45} & y_{46} \\ y_{50} & y_{51} & y_{52} & y_{53} & y_{54} & y_{55} & y_{56} \\ y_{60} & y_{61} & y_{62} & y_{63} & y_{64} & y_{65} & y_{66} \end{bmatrix} \times \begin{bmatrix} v_0 \\ v_1 \\ v_2 \\ v_3 \\ v_4 \\ v_5 \\ v_6 \end{bmatrix}. \quad (3)$$

Because of the symmetric structure of the ESPAR antenna

$$\begin{aligned} y_{11} &= y_{22} = y_{33} = y_{44} = y_{55} = y_{66} \\ y_{01} &= y_{02} = y_{03} = y_{04} = y_{05} = y_{06} \\ y_{12} &= y_{23} = y_{34} = y_{45} = y_{56} = y_{61} \\ y_{13} &= y_{24} = y_{35} = y_{46} = y_{51} = y_{62} \\ y_{14} &= y_{25} = y_{36}. \end{aligned}$$

Therefore, the admittance matrix $\mathbf{Y}$ is described with only six parameters. These values are obtained with the Numerical Electromagnetic Code (NEC). The voltages on the active central monopole and the mth parasitic monopole are represented by (4) and (5), respectively

$$v_0 = v_s - z_0 i_0 \quad (4)$$

$$v_m = -jx_m i_m \quad (5)$$

where $m = 1, \ldots, 6$. z_0 is the characteristic impedance of 50 Ω at the RF port. v_s represents the transmitted voltage signal source with the amplitude and the phase from the driving RF port at the central element. Write (4) and (5) into a matrix form as follows:

$$V = \begin{bmatrix} v_s \\ 0 \\ 0 \\ 0 \\ 0 \\ 0 \\ 0 \end{bmatrix} - \mathbf{X}I = v_s U_1 - \mathbf{X}I \quad (6)$$

and define

$$\mathbf{X} = \text{diag}[z_0, \quad jx_1, \ \ldots, \quad jx_6] \quad (7)$$

where

$$U_1 = [1 \quad 0 \quad 0 \quad 0 \quad 0 \quad 0 \quad 0]^T. \quad (8)$$

Combining (3) and (6), we obtain

$$I = \mathbf{Y}V = \mathbf{Y}(v_s U_1 - \mathbf{X}I). \quad (9)$$

After a simple mathematical manipulation, we can obtain

$$I = v_s(\mathbf{Y}^{-1} + \mathbf{X})^{-1} U_1 = v_s W \quad (10)$$

where $(\mathbf{Y}^{-1} + \mathbf{X})^{-1} U_1$ is represented as W, a 7-by-1 vector, called an *Equivalent Weight Vector*. The far-field radiation pattern is the superposition of all monopoles' radiation patterns [21]. Therefore, the far-field current signal in the azimuthal direction θ with its amplitude and the phase is represented as

$$y(\theta)_{\text{far}} = I^T \alpha(\theta) = W^T \alpha(\theta) v_s. \quad (11)$$

The steering vector $\alpha(\theta)$ is defined based on the array geometry (see Fig. 3)

$$\alpha(\theta) = \begin{bmatrix} 1 \\ e^{j\frac{\pi}{2}\cos(\theta)} \\ e^{j\frac{\pi}{2}\cos\left(\theta - \frac{\pi}{3}\right)} \\ e^{j\frac{\pi}{2}\cos\left(\theta - \frac{2\pi}{3}\right)} \\ e^{j\frac{\pi}{2}\cos(\theta - \pi)} \\ e^{j\frac{\pi}{2}\cos\left(\theta - \frac{4\pi}{3}\right)} \\ e^{j\frac{\pi}{2}\cos\left(\theta - \frac{5\pi}{3}\right)} \end{bmatrix}. \quad (12)$$

According to the reciprocity theory for radiation patterns [21], if the antenna is working in the receiving mode, the voltage signals $u(t)$ at the RF port are

$$u(t) = W^T \alpha(\theta) s(t) \quad (13)$$

where, $s(t)$ represents the far-field incident current waves with the amplitude and the phase in the azimuthal θ direction. W in (13) is dependent on the reactance at each parasitic monopole. Desired beam patterns could be formed by tuning the reactances $(x_1, x_2, \ldots, x_6)$. This is achieved by changing the control voltages $(Vcc_1, Vcc_2, \ldots, Vcc_6)$ of the diodes, which are connected to parasitic elements.

Note that (13) has the same form as the beamforming equation in array processing literatures [22], [23]. Signals received at the antenna receiver are the sum of the *weighted* signal samples at individual antenna sensor elements.

For beamforming based on conventional DBF array antennas, signal samples are obtained at the baseband, and the desired output is the linear combination of these samples. If the objective function is the minimum square error (MSE) between the training signals and the combined output, the beamforming is a Wiener filtering problem. The optimum solution of the combining weight is obtained by solving the Wiener–Hopf equation [22], [24]. To reduce the computational complexity, the linear mean square (LMS) algorithm is employed to obtain the optimum solution through iteration using the gradient of the MSE objective function which is in a linear quadratic form [24]. On the contrary, the ESPAR antenna has only one RF port. Signals impinging on the antenna elements are combined due to the strong mutual coupling. The baseband receiver receives the combined signals from the sole RF port. This combining is nonlinear as seen from the above equations.

Furthermore, for the DBF array antennas, the optimum *weight* obtained is multiplied with the signal sample vector digitally at the baseband. For ESPAR antennas, the *weight* is tuned by changing the reactance values at antenna elements based on a nonlinear relationship between the control voltages and the beam pattern. Therefore, W defined in (10) is called the *equivalent weight vector*. This unique property of the ESPAR antenna initiates our design of the adaptive beamforming algorithm based on a numerical iterative manner as for a nonlinear filtering problem.

B. Signal Model and Assumption

To model the propagation environment and simulate the adaptive beamforming of an ESPAR antenna, we assume a line-of-sight (LOS) propagation environment, and the multipath components are not considered. These assumptions give a direct insight into the beamforming ability of the ESPAR antenna.

Signals are assumed to come in the azimuth plane. When there are total K signals impinging on the antenna, the received RF signal $y(t)$ is the sum of all the RF signals from individual signal sources

$$y(t) = \sum_{k=1}^{K} W^T \alpha(\theta_k) s_k(t) + n(t) \tag{14}$$

where θ_k is the azimuthal angle of the kth impinging signal. $n(t)$ is the added white Gaussian noise (AWGN) component with the power of σ^2. $s_k(t)$ denotes the kth signal wave impinging on the antenna array.

III. Adaptive Beamforming Algorithm

As aforementioned, the optimum *weight* has to be obtained numerically. The objective function of the iteration process is the normalized mean square error (NMSE) between the received signal and the desired signal (reference signal). It is simply represented by $1-|\rho_{yd}|^2$, where ρ_{yd} is the cross correlation coefficient (CCC) between the desired and the received signals [16]. ρ_{yd} is expressed as follows:

$$\rho_{yd} = \frac{E\left[y(t)r(t)^*\right]}{\sqrt{E\left[y(t)y(t)^*\right]E\left[r(t)r(t)^*\right]}} \tag{15}$$

where $r(t)$ is the reference signal. The superscript * represents the complex conjugate. Since the objective function is based on the CCC, and the goal of the iteration is to maximize the CCC to minimize the NMSE, we also call this algorithm a maximum CCC (MCCC) algorithm. The output SINR is approximately represented by $|\rho_{yd}|^2/(1-|\rho_{yd}|^2)$. In this optimization problem, the system parameters are the reactance values, which are controlled by the RB voltages $(Vcc_1, Vcc_2, \ldots, Vcc_6)$ at tunable varactors. The desired beam pattern is obtained by changing the reactance values through iterations.

The reported algorithm [15] is based on the steepest gradient method [25], a classical deterministic optimization method. It assumes that one knows exactly the loss function (and its derivatives if relevant) and that information is used to calculate the gradient of the optimization search route in a deterministic manner at each step of the iteration. (Perturb each parameters of the system; measure the loss function; and determine the gradient with respect to each individual parameter.) This is not computationally efficient if the system has a considerable amount of parameters. As for the seven-element ESPAR antenna, there are six parameters (load reactances at six parasitic elements). This algorithm hinders us to implement more parasitic elements to improve the performance and impedes the reduction of the iteration process. Furthermore, we do not have the perfect information about the loss function, because the measurement of the loss function is quite *noisy*. This *noise* denoted by ε in following equations is not the AWGN, rather it is the randomness and the inevitable error in observing the loss function [26]. For example, we cannot compute the *mean* square error. In practice, it is a squared error over a finite length of observations. In our algorithm the observation length of the loss function is 50-data bits. Therefore, the optimization process of the ESPAR antenna should be modeled more properly as the stochastic optimization problem, especially in the Kiefer–Wolfowitz setting [26], in which one uses only *noisy* measurements of the objective function to estimate the gradient of the objective function.

A. Procedure of the Optimization

The objective function is the NMSE. It is represented as

$$L\left(X(n)\right) = 1 - |\rho_{yd}|^2 \tag{16}$$

where $X(n)$ is the reactance values $(x_1, x_2, \cdots, x_6)$ at the nth iteration stage. ρ_{yd} is the CCC between the received signal and the reference signal. The estimated gradient of the optimization problem is

$$\widehat{g_n} = \frac{\left(\widehat{L_n^{(+)}} - \widehat{L_n^{(-)}}\right)}{2c(n)\triangle_n}. \tag{17}$$

The $\widehat{\ }$ denotes estimated values. $\widehat{L_n^{(\pm)}}$ is the estimated value of the objective function with the parameters (six reactance values) simultaneously perturbed to the positive and negative directions, respectively, at the nth iteration

$$\widehat{L_n^{(\pm)}} = L\left(X(n) \pm c(n)\triangle_n\right) \pm \varepsilon^{(\pm)} \tag{18}$$

$$\triangle_n = \left[\triangle_n^{(1)} \quad \triangle_n^{(2)} \quad \triangle_n^{(3)} \quad \triangle_n^{(4)} \quad \triangle_n^{(5)} \quad \triangle_n^{(6)}\right]. \tag{19}$$

Each entity is selected based on the Bernoulli distribution. Their values are either 1 or -1 with a probability of 1/2 [27]. $c(n)$ is the perturbation size at the nth iteration

$$c(n) = \frac{C}{(n+1)^{\gamma}} \tag{20}$$

where C is a constant. ε is the *noise* component as aforementioned. Please note that, although the observation of the loss function is a scalar, g_n is a vector with six entities. New reactance values are updated as follows:

$$X(n+1) = X(n) - a(n)\widehat{g_n} \tag{21}$$

where, $a(n)$ is the updating step size, a and A are the constants, and α and γ are nonnegative coefficients

$$a(n) = \frac{a}{(A+n+1)^{\alpha}}. \tag{22}$$

Only two measurements of the loss function are needed to get the gradient g_n. This is obviously because all the parameters are always perturbed together instead of one by one as in the steepest gradient optimization process [15], [25]. The step size goes to zero as $n \to \infty$. This character allows an average on the *noise* in the long run [26]. $c(n)$ also follows $\sum_{n=0}^{\infty} c(n) = \infty$ to satisfy the convergence condition.

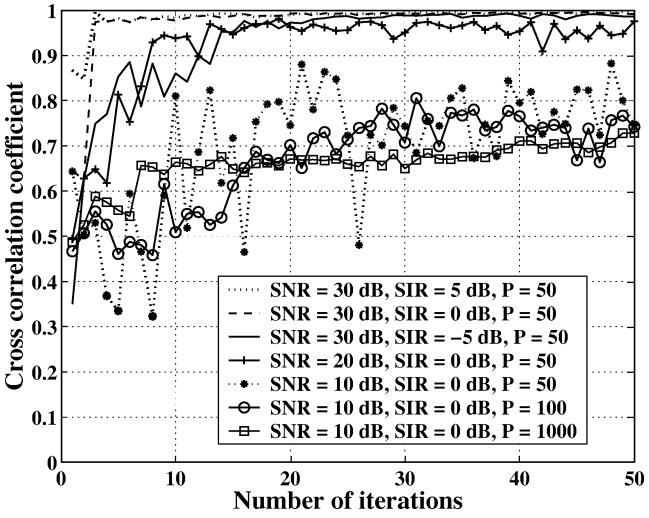

Fig. 4. Cross correlation coefficient between the received signal and the training signal in different environment settings for the proposed ESPAR SPSA beamforming algorithm. The azimuthal DOAs of one desired signal and one interference signal are 0° and 90°, respectively.

B. Selection of Parameters

In this paper, we select the values of α, γ, C, and a from [27]. It was recommended to choose α and γ as 0.602 and 0.101, respectively (practically effective and theoretically valid). C is set at the level approximately equal to the standard deviation of the measured noise in the objective function. a is selected together with A while satisfying that the magnitude of the gradient times $a/(A+1)^{\alpha}$ approximately equals to the smaller perturbation size of the parameters in the early iterations. In our design, the parameters are the control voltages $(Vcc_1, \ldots, Vcc_6)$ at the tunable reactances. We selected 50 as the maximum number of iterations in the algorithm, because it is not too long, but is sufficient for the algorithm to converge.

Although the selection of parameters is based on the guideline in [27], in the experiment we cannot directly use the parameters that are optimal to simulation environment as differences between two systems exist. The practical parameters have to be selected through trials and errors. In our system, we set a =8002000, C =280, A =100.

IV. Simulation Results and Discussion

A. Speed of Convergence

In the simulation the DOA of the desired signal is set 0°. The length of each data sample block P is 50 bits. The total number of iterations N is 50. For the proposed algorithm based on SPSA, the total length of training signals required is $P \times 2 \times N$ [27]. Based on the varactor catalog data [28], we model the relationship between the digital control voltage Vcc_i and the reactance x_i $(i = 1, \ldots, 6)$ with a linear equation

$$x_i = -0.0217\, \mathrm{V}cc_i - 49.21. \tag{23}$$

First, we study the convergency of the algorithm. The interference is impinging on the antenna from 90°. We set the signal-to-noise-ratio (SNR) as 30 dB and vary the signal-to-interference-ratio (SIR) from 5 to −5 dB. Second, we vary the SNR keeping the SIR at 0 dB. The learning curves of CCCs for different settings are plotted in Fig. 4.

TABLE I
Averaged Simulation Results (Averaged Over Ten Times of Executing the Program) for Different Environment Settings. $P = 50$. $N = 50$. DOAs of One Desired Signal and One Interference Are 0° and 90° in the Azimuth Plane, Respectively. (Results in the Shaded Region Are Obtained When $P = 1000$)

SIR (dB)	SNR = 30 dB	
	Output SINR (dB)	Formed Null (dB)
-5	15	24
0	16	21
5	18	17

SNR (dB)	SIR = 0 dB	
	Output SINR (dB)	Formed Null (dB)
10	2	16
20	10	17
30	16	21

When we fix the SNR at 30 dB and vary the SIR from 5 to −5 dB, the algorithm converges to a point where the output SINR is more than 15 dB. At the beginning of the iteration, the value of ρ_{yd} is influenced by the input SIR. When the SIR is kept at 0 dB and we lower the SNR to 20 dB, ρ_{yd} still reaches more than 0.95 (solid line with plus signs), which corresponds to an output SINR of 10 dB. However, the algorithm could not converge when the SNR is ≤10 dB. In a high noise level environment (SNR ≤10 dB), it is difficult to estimate correctly the CCC between the training signals and the received signals with only 50 bit samples. To ensure a correct calculation of the CCC, the sample length P needs to be increased. In Fig. 4 the CCCs with 100-bit and 1,000-bit block samples are plotted, respectively.

We also note that the performance of the algorithm varies at each time. This is because of the randomness of the CCC between the shot training signal and the signals transmitted by the interference. Their correlation is varying randomly rather than being zero. This phenomenon is also observed in other experiments and field tests [29]–[31]. Averaged results for different environment settings are listed in Table I. Simulation shows that 50 iterations are more than sufficient for the algorithm to converge.

B. Comparison With Standard LMS Beamforming

To give a comparison on the convergence of the proposed beamforming algorithm with the standard LMS beamforming algorithm based on DBF array antennas of the same array geometry of the seven-element ESPAR antenna, we plot the learning curve of the LMS algorithm in Fig. 5. The mutual coupling of the array antenna is also considered. The length of each data sample block is 50 bits. The step size is 0.07. From the figure we can see that the LMS beamforming algorithm requires comparatively less iterations to achieve the same CCC (the same output SINR). However, the penalties are the storing of seven times the data as for the ESPAR beamforming algorithm and the increase of the computational complexity. Needless to say the complexity of the circuit and the power consumption as aforementioned.

C. Null Forming Ability

To justify the null forming ability of the proposed algorithm, the formed beam patterns are also plotted in Fig. 6. We observe that the algorithm still forms deep nulls even when the interference level increases. This is because that the CCC between the

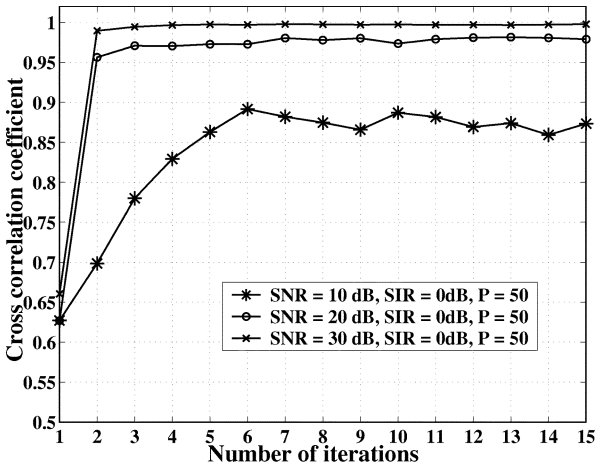

Fig. 5. Cross correlation coefficient between the received signal and the training signal for LMS adaptive beamforming algorithm. The azimuthal DOAs of one desired signal and one interference signal are 0° and 90°, respectively. The length of each data sample block is 50 bits. The step size is 0.07.

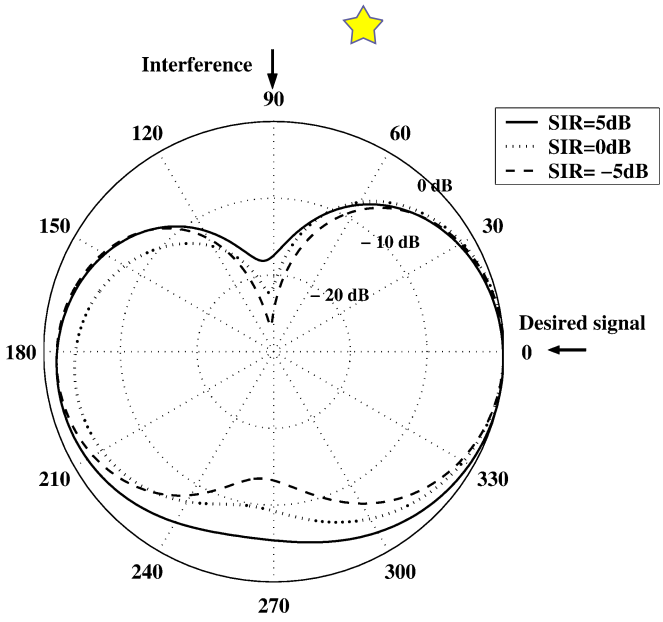

Fig. 6. Averaged ($P = 1000$) simulated beam patterns (normalized gain in decibels) in the azimuth plane for different SIRs. SNR = 30 dB.

received signals and the training signals is mostly influenced by the interference instead of the AWGN. While the MCCC based algorithm is searching to maximize the CCC, the interference is getting suppressed.

We also set the azimuthal DOAs of the interferer at 180°, 225°, and 315°, respectively, while keeping the DOA of the desired signal at 0°. The averaged results are produced in Table II. Among four cases, the performances are the best when the interferer is at 90° or 225°. This could be explained by examining the spatial correlation between the ESPAR steering vector for the desired signal's direction θ_1 and the one for the interferer's direction θ_2. The spatial correlation coefficient at the ESPAR antenna is plotted in Fig. 7, where the DOA of the desired signal is fixed at 0°, the DOA of the interferer is changing from 0° to 360°. The performance degrades when the angular separation

TABLE II
SIMULATION RESULTS (AVERAGED OVER TEN TIMES OF EXECUTING THE PROGRAM) FOR DIFFERENT DOAS IN THE AZIMUTH PLANE OF THE INTERFERENCE SIGNAL. DOAS OF THE SIGNAL OF INTEREST IS 0°

Interferer's direction in the azimuth plane		90°	180°	225°	315°
SNR 20 dB	Output SINR (dB)	10	8	9	6
	Formed Null (dB)	17	15	16	11
SNR 30 dB	Output SINR (dB)	18	11	14	11
	Formed Null (dB)	22	14	18	13

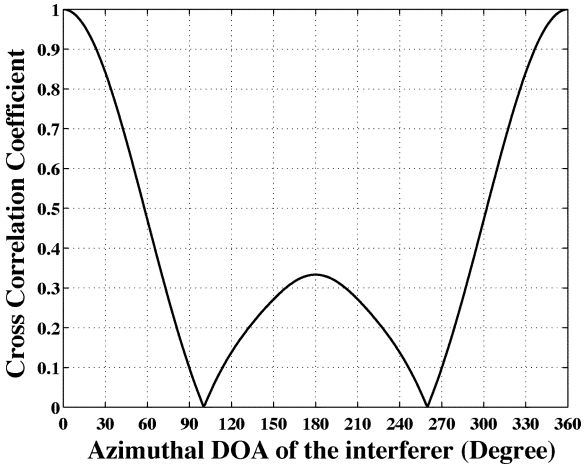

Fig. 7. Spatial correlation coefficients at the ESPAR antenna between the desired signal ($\theta_1 = 0°$) and the interference signal at different azimuthal angles (θ_2 is from 0° to 360°).

between the desired signal and the interference is getting small. The received signals at the RF port could be represented as

$$y(t) = W^T \left(s_1(t)\alpha(\theta_1) + s_2(t)\alpha(\theta_2)\right) + n(t). \qquad (24)$$

Analogous to the duplicate channel in user division in a space division multiple access (SDMA) scheme [32], [33], the less spatial correlation between the desired signal and the interference signal is, the better the null forming to the interference.

Finally we increase the number of interferers to two. The powers of the interference signals are equally set to be half of the desired signal's power. Therefore, the SIR is kept 0 dB. The SNR is set to be 30 dB. Directions of two interferers are 90° and 270° in the first case, and 225° and 270° in the second case. Averaged results over ten times of executing the algorithm are listed in Table III. Although the performances with respect to the output SINR and the formed null degrade around 2 dB comparing to the same condition with one interferer, more than 10-dB nulls are still formed at the interferers' directions. Beam patterns for the two cases when the SNR is 20 dB are plotted in Fig. 8.

Simulation studies show that the proposed algorithm is more efficient to combat against the interference than to the noise. Therefore, the algorithm is suitable and sufficient for the interference dominant environment, for example in ad hoc network applications where the link quality and throughput at a

TABLE III
SIMULATION RESULTS (AVERAGED OVER TEN TIMES OF EXECUTING THE PROGRAM) WHERE THERE ARE TWO INTERFERERS. CASE I: INTERFERERS' DIRECTIONS ARE 90° AND 270°. CASE II: INTERFERERS' DIRECTIONS ARE 225° AND 270°. DOA OF THE DESIRED SIGNAL IS 0°

	SNR (dB)	Formed null at interferer 1's direction (dB)	Formed null at interferer 2's direction (dB)	Output) SINR (dB)
Case I	20	15	13	9
	30	16	16	15
Case II	20	14	6.5	8
	30	17	10	12

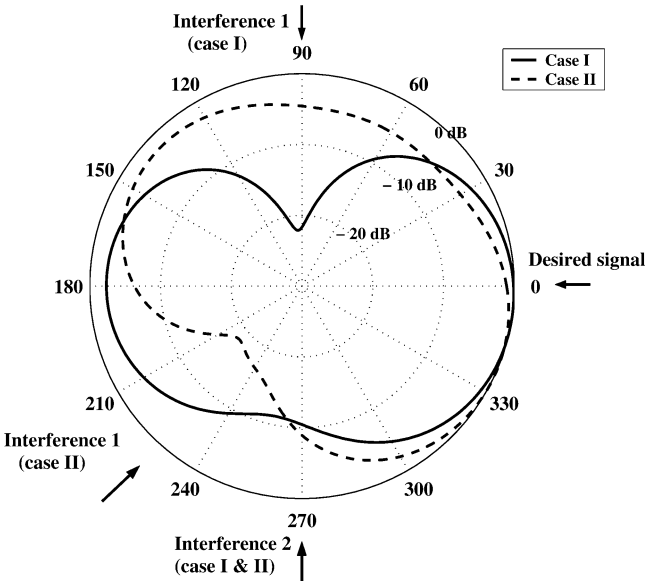

Fig. 8. Simulated beam patterns (normalized gain in decibels, $P = 1000$) in the azimuth plane when there are two interferers. $\mathrm{SIR} = 0$ dB. $\mathrm{SNR} = 30$ dB. $N = 50$. Case I: Interferers' directions are 90° and 270°. Case II: Interferers' directions are 225° and 270°.

node are mainly limited by the interferences from the neighboring nodes (mobile terminals). In a moderate condition (SNR is around 20–30 dB), the algorithm could achieve an output SINR of around 10 dB within a few iterations. Thus, a sound link (BER $\leq 10^{-3}$) could be established quickly.

V. EXPERIMENT TESTBED

To justify the proposed adaptive beamforming algorithm, the ESPAR antenna testbed was set up in an anechoic chamber. The functional block diagram of the testbed is shown in Fig. 9. It consists of a transmitter block, a receiver block, a baseband digital block, and the antenna motor control block (not shown in the figure).

A. Transmitter and Receiver Setup

The data, a 13th-order m-sequence is generated at the field programmable gate arrays (FPGAs) m-sequence generator-1 and generator-2 for the transmitter and for generating reference signals at the receiver, respectively. The inner signal reference certifies that two generators produce the same sequence. At the transmitter part, with this m-sequence as modulating signals the vector signal generator produces a binary phase shift keying (BPSK) RF signal at 2.484 GHz, the channel-14 in IEEE 802.11b WLAN protocols. Signals are transmitted with a 17 dBi horn antenna (Scientific Atlanta Standard Horn antenna. Model: 12–17.0) pointing to the ESPAR antenna. It is about 5 m above the ground floor. The SNR is adjusted by tuning the power of the transmitter's signal.

The ESPAR antenna, as the receiving antenna, is mounted on a test positioner. The received signals of the ESPAR antenna pass through a low-noise amplifier (LNA). The amplified signals are directly down-converted to 70-MHz intermediate frequency (IF) signals at the mixer with a 2.414-GHz local oscillator signal. After passing through the second amplifier and the bandpass filter (BPF), the signals are splitted into in-phase (I) and quadrature (Q) components. Two ADCs (500 kHz sampling rate) simultaneously convert the I and Q components into 12-bit digital signals.

In our experiment, the interference is randomly generated by the signal generator and is transmitted with a 14 dBi Yagi–Uda antenna (WLE-HG-DYG Yagi). The SIR is tuned by adjusting the power of the interference signals. The interference signal's DOA is set by placing the Yagi–Uda antenna at different places in the anechoic chamber.

B. Baseband Digital Block

Sampled digital signals from the A/Ds of the I/Q channel are sent to the TMS320C6701 DSP chip, where the algorithm is carried out. With the reference signals, the CCC between the received signals and the reference signals ρ_{yd} is calculated and displayed on the computer control panel. The DSP chip outputs the updated reactance 12-bit digital control voltages ranging from 2047 to −2048 (decimal value of the 12-bit binary digit). Six D/A converters generate analog control voltages $(Vcc_1, Vcc_2, \ldots, Vcc_6)$ from 20 to −0.5 V correspondingly.

The reference signal and the received signal from the I/Q channels are displayed on the oscilloscope for a real time monitoring. The CCC, the received signal, the reference signal and the control voltages of the load reactances are saved for postprocessing. For calculating the gradient at each iteration stage, the training signals should be the same when perturbing the parameters to the positive and negative directions. This is achieved by setting a *guard time* on the FPGAs generated 13th-order m-sequence. Since we use 50-bit signal samples to calculate the CCC ρ_{yd}, our guard time is $2^{13}-1-$ 50 bits. The DSP chip waits during the guard time until it gets the same 50-bit prefix of the 13th-order m-sequence. Fig. 10 illustrates this implementation.

Due to the hardware limitation, we set a relatively long time for DSP processing and D/A conversion. This eliminates the influence from the hardware processing delay and assures that we get exactly the same training signals for the gradient calculation during the experiment stage. For real implementations with high speed D/A converters and DSP chips, the *guard time* could be greatly reduced to a few bit duration.

C. Implementation of the Algorithm

When implementing the algorithm, the hardware limitations need to be considered. For our fabricated ESPAR antenna, two diodes (1SV287, V_R : − 20 to 0.5 V, C: 0.7–9.0 pF, Cmax/Cmin is 7.6 at 1 MHz) positioned in parallel terminate at each parasitic monopole. The analogue control voltages Vcc (from 20 to

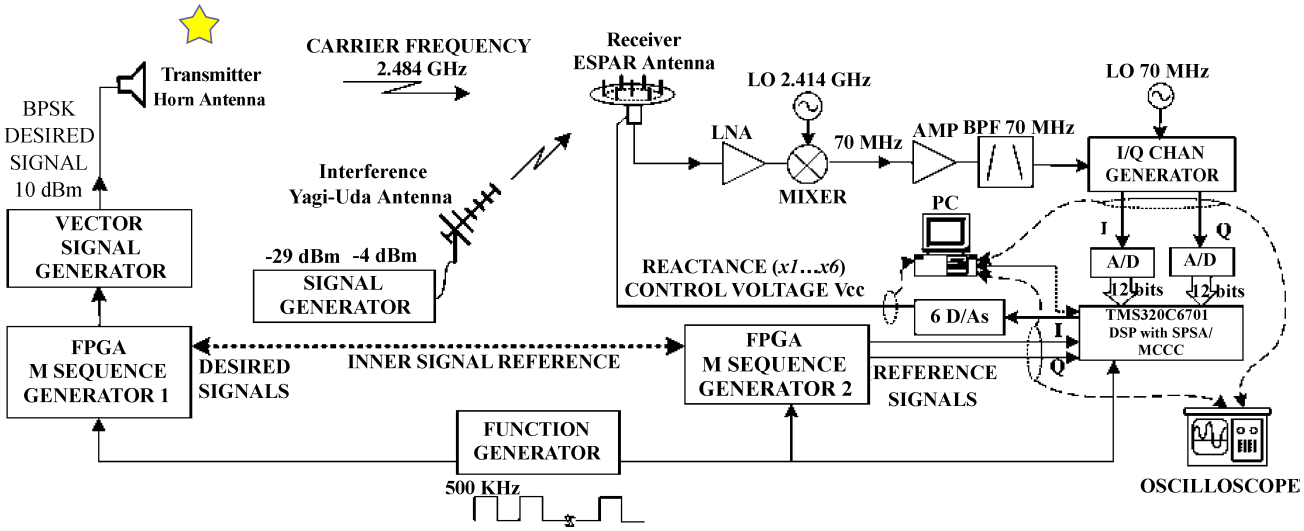

Fig. 9. ESPAR adaptive beamforming algorithm experiment testbed functional block diagram.

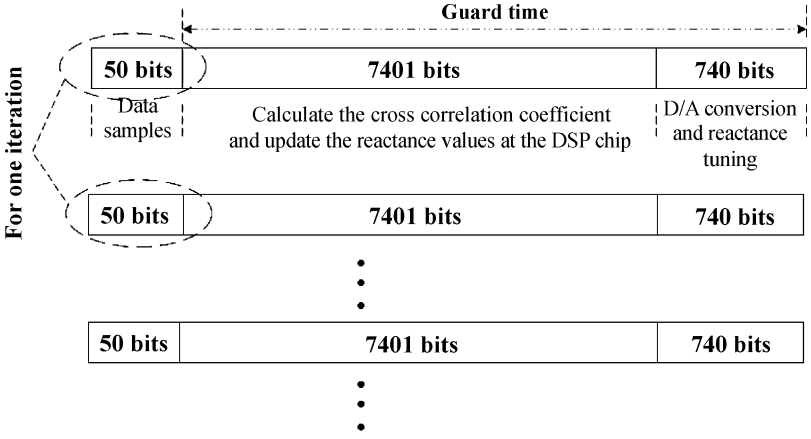

Fig. 10. Setting of the guard time at DSP chip. For each iteration, 50 × 2 bits are required to calculate the gradient.

−0.5 V) impress on reverse polarities of the diodes (see Fig. 11) to make them reverse biased. The two parallel diodes are tuned to function as one tunable reactance that gives a reactance from $-45.8j\ \Omega$ to $-3.6j\ \Omega$. The reactance value cannot be tuned over a wide range, because of the physical limitation of the diode and the constraint imposed on the input impedance of the RF port.

The beam steering of the ESPAR antenna is based on the strong coupling among the active center element and six varactor loaded parasitic elements. The impedance and the resonant frequency of the elements vary as the beam pattern is tuned. This may lead to an unacceptable level of input return loss (S_{11}) for practical applications. A constraint is imposed on the practical range that is from $-45.8j\ \Omega$ to $-3.6j\ \Omega$. The corresponding digital control voltage (decimal value of 12-bit binary representation of analog control voltage from 20 to −0.5 V) is from 2047 to −2048. Within the range the antenna has −10 dB return loss (S_{11}) bandwidth of 30 MHz centered at the desired resonant frequency as the beam pattern is tuned over 360° in the azimuth plane [34]. This proves that the antenna does not suffer significant scan blindness.

The constraint on the range of the tunable reactances at the parasitic elements is achieved by adding two limits on the control voltages in the algorithm implemented at the DSP board.

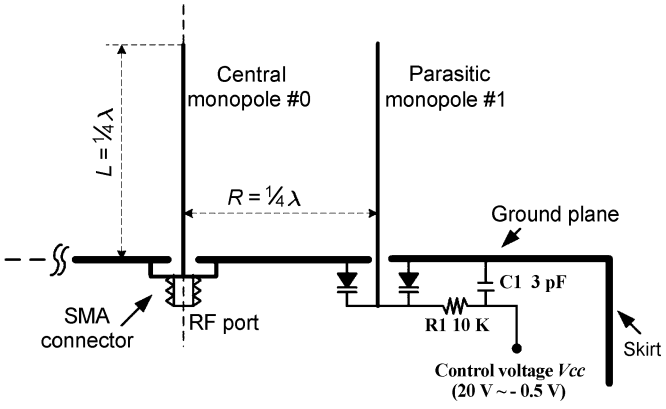

Fig. 11. Vertical cross section view of the ESPAR antenna and a reactance circuit of one of the six parasitic elements [19]. The length of each monopole is one-quarter wavelength $(\lambda/4)$ of the transmitting RF signal with the frequency of 2.484 GHz.

One constraint is just before the measurement of the loss function with the perturbation. When the program generates the random Δ_n and perturbs the reactances to the positive direction, the program checks the resulted reactance values. In case any reactance is beyond the range, that reactance is resumed to

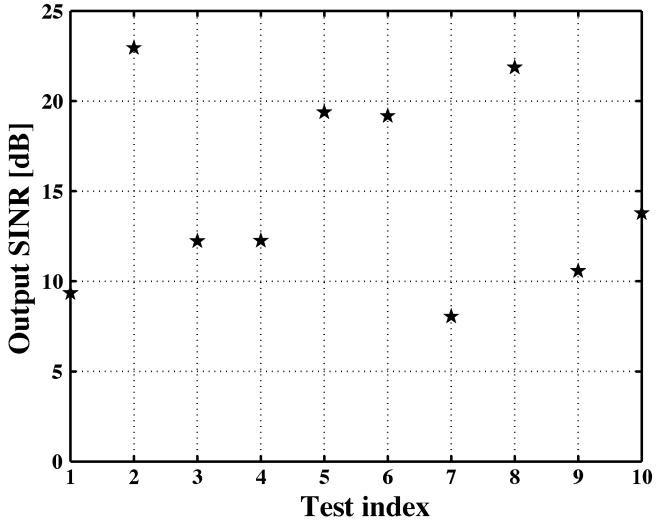

Fig. 12. Output SINRs for ten tests. The average output SINR is 15 dB. The standard deviation is 5.4 dB.

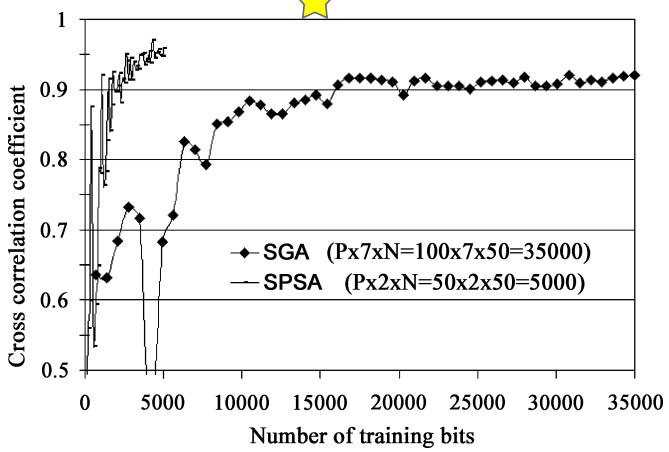

Fig. 13. Comparison between the SGA beamforming algorithm and the SPSA beamforming algorithm over number of training bits. For the SPSA beamforming algorithm, the CCC converges to 0.96 within $P \times 2 \times N = 50 \times 2 \times 50 = 5000$ bits. For the SGA beamforming algorithm, the number of the training signals is $\mathrm{P} \times 7 \times \mathrm{N} = 100 \times 7 \times 50 = 35\,000$ bits.

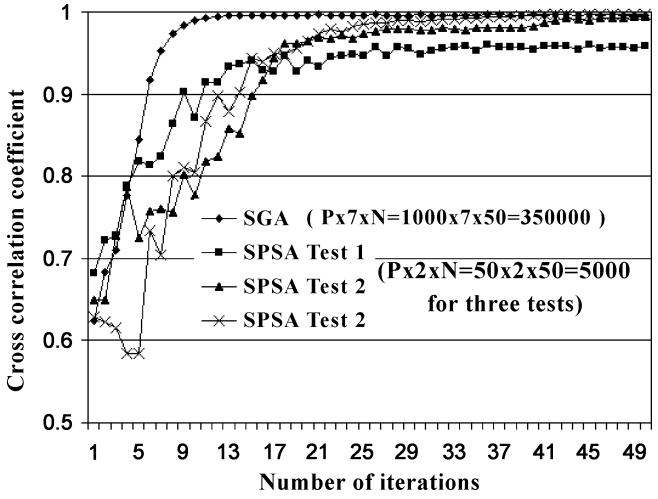

Fig. 14. Comparison between the SGA beamforming algorithm and the SPSA beamforming algorithm over the number of iterations. $N = 50$ for both algorithms. For the SPSA beamforming algorithm, $P = 50$. The total number of training bits is $P \times 2 \times N = 5000$. For the SGA beamforming algorithm, $P = 1000$. The total number of training bits is $P \times 7 \times N = 350\,000$.

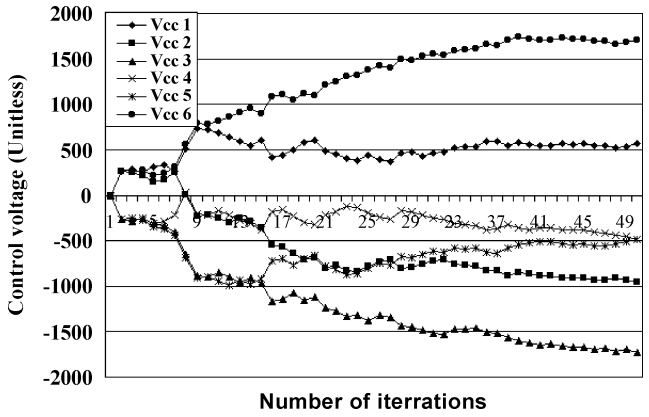

Fig. 15. Learning curves of the control voltages $(Vcc_1, \ldots, Vcc_6)$ [decimal value (2047 to -2048) of 12-bit binary representation of analog control voltage (20 to -0.5 V)]. The cross correlation coefficient reaches 0.98. The output SINR is 13 dB.

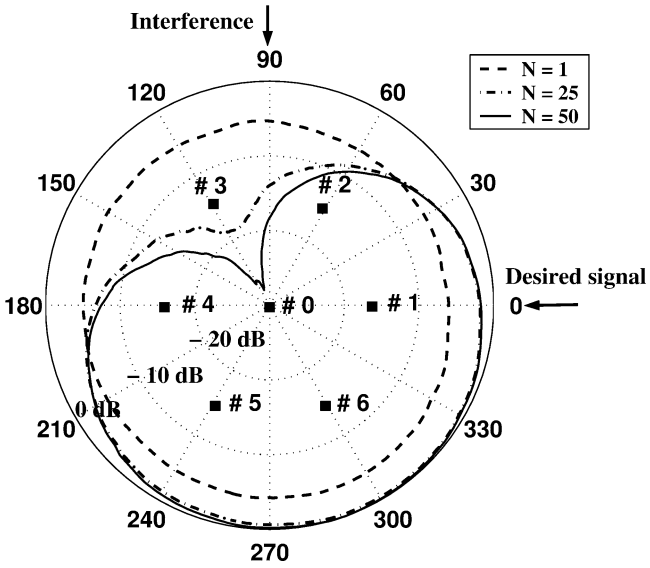

Fig. 16. Formed successive beam patterns at different iteration stages (normalized antenna gain in decibels). The formed null is around 19 dB. The CCC reaches 0.98. The output SINR is 13 dB. $P = 50, N = 50$. (♯—positions of seven elements in an ESPAR antenna.).

the initial value before the perturbation. The same check procedure is carried out for the perturbation to the negative direction. The maximum perturbation size is always smaller than the range of the reactance. In another word, each reactance value is within the range at least for one perturbation. The gradient with respect to $X(n)$ is obtained with one measurement of the loss function with the perturbed parameters and one without the perturbation as in (17) [27]. This is also a valid estimation of the gradient [27]. Another constraint is imposed on the updating of the reactance values $X(n)$. If the updating of the reactances results in a value exceeding the range, the parameter is assigned the boundary value.

VI. Experimental Results

In this section, we discuss the results of the experiment carried out in a radio anechoic chamber. The placements of the test equipments are shown in Fig. 9. The transmitter horn antenna, the receiver ESPAR antenna and the interference generating

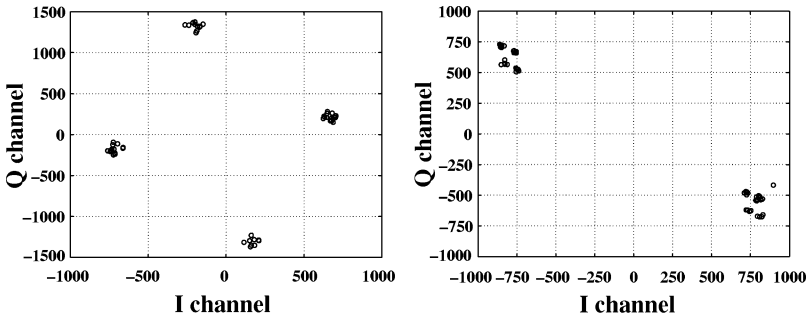

Fig. 17. BPSK signal constellations (a) at the beginning and (b) the end of the iterations. The cross correlation coefficient reaches 0.98. The output SINR is 13 dB.

Yagi–Uda antenna are placed in the same height level. Signals are assumed to be in the same azimuth plane. The number of iterations is 50 ($N = 50$). The length of the data sample block is 50 bits ($P = 50$). Therefore, the length of total training signals is $P \times 2 \times N = 5000$ bits. The SNR at the chamber is set at 20 dB, whereas the SIR is kept 0 dB. The DOA of the desired signal is always 0°.

In the first test, the interference is coming from 90° in the azimuth plane. The output SINRs for ten tests are shown in Fig. 12. In most cases, the output SINR exceeds 10 dB. The average output SINR is around 15 dB. Results exhibit a standard deviation of 5.4 dB. This is due to the short data sample block used to calculate the correlation coefficient as we have mentioned in the previous section. One learning curve of the test is plotted in Fig. 13. In this case, the CCC ρ_{yd} reaches 0.96. The corresponding output SINR is 11 dB.

We also compare the proposed algorithm with an ESPAR antenna beamforming algorithm [15] which employs the well-known steepest gradient algorithm (SGA) [25]. The CCC curves for both algorithms are plotted in Fig. 13. For the proposed algorithm, we set $P = 50$. For the beamforming algorithm with SGA, we set $P = 100$. These values are the experimentally tested minimum length of data sample block for each algorithm to be stable. The reason why the SPSA beamforming algorithm could use much shorter observation sample block is that the effect of the *noise* which is the randomness of the observation of the objective function is eliminated by allowing the parameter updating step size [see (22)] to go to zero as $n \to \infty$ [26]. While for the classical deterministic SGA, it is kept constant [15], [25].

With the same number of iteration ($N = 50$), the proposed algorithm uses $P \times 2 \times N = 50 \times 2 \times 50 = 5000$ bits, while the SGA beamforming algorithm uses $P \times 2 \times N = 100 \times 7 \times 50 = 35\,000$ bits. If the number of training signals for SGA beamforming ($P \times 7 \times N$) is limited to around 5000 bits, N has to be set 8 with $P = 100$. As shown in the figure, within roughly the same length of training bits, it could not converge. This is because eight observations of the objective function are required to calculate the gradient at one iteration [15]. With a limited number of training bits, the algorithm cannot converge within a few iterations.

However, the beamforming algorithm with SGA converges to the optimal point within 50 iterations if a long training signal is available. Because the *noise* effect is eliminated by using longer data sample block, for example 1000 bits. In Fig. 14, the performances of the SGA beamforming algorithm and the proposed SPSA beamforming algorithm are compared using the same number of iterations. From the figure, we could observe that SGA converges to the optimal point. But the total number of

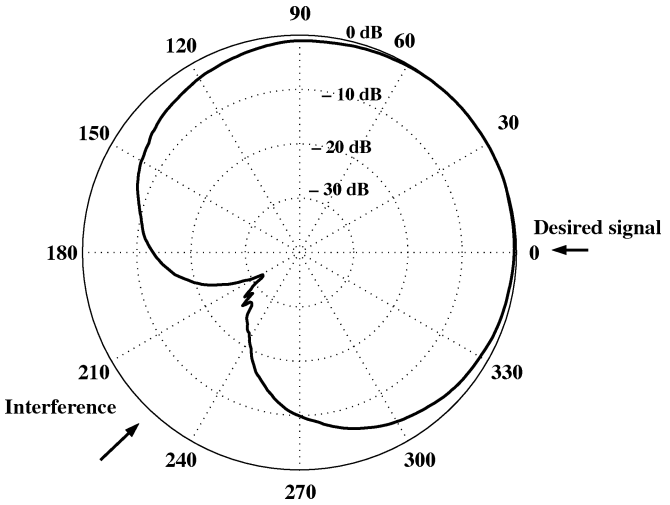

Fig. 18. Measured azimuthal beam pattern ($P = 1,000$). DOAs of the desired signal and one interference signal are 0° and 225°, respectively.

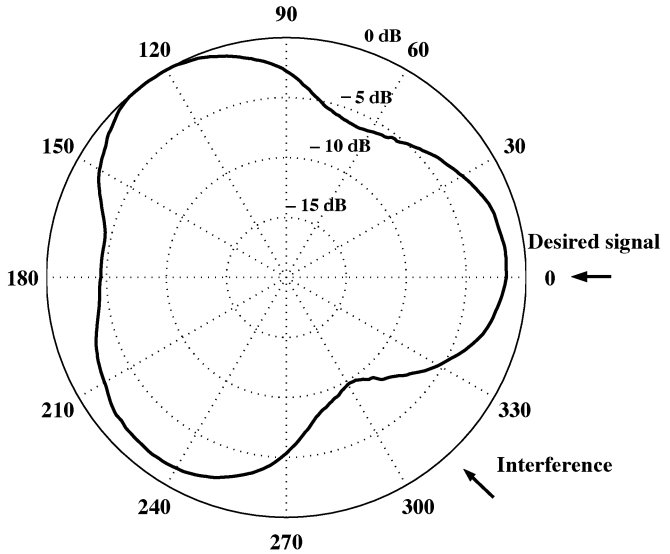

Fig. 19. Measured azimuthal beam pattern ($P = 1,000$). DOAs of the desired signal and one interference signal are 0° and 315°, respectively.

TABLE IV
AVERAGED DIGITAL CONTROL VOLTAGES. (DECIMAL VALUE OF THE 12-BIT BINARY DIGITAL VALUE) AFTER CONVERGENCE AND THE AVERAGED PERFORMANCE WITH $P = 1000$ (BITS). (THE DIGITAL VOLTAGE, RANGING FROM 2047 TO -2048, IS ASSOCIATED TO THE ANALOG BIAS VOLTAGE FROM 20 TO -0.5 V)

Interference(s)' azimuthal direction	Vcc_1	Vcc_2	Vcc_3	Vcc_4	Vcc_5	Vcc_6	Output SINR (dB)	Standard Deviation (dB)	Formed Null (dB)
90°	-48	-1322	-1530	-760	362	1506	15	5.4	19
225°	609	1105	-295	-1353	-1665	-681	14.5	5.6	24
315°	-685	929	-1503	1007	-1419	-623	6	1.4	7
90° & 270°	740	188	-1378	-322	-1344	736	3.7	1.1	7 & 3
225° & 270°	633	1663	-551	-807	-1641	-543	6.6	1.7	15 & 10

training signal bits is $P \times 7 \times N = 1000 \times 7 \times 50 = 350\,000$. This could be impractical for real applications.

The digital control voltages $(Vcc_1, \ldots, Vcc_6)$ for one test of the proposed algorithm at different iteration stages are plotted in Fig. 15. The forming of the null with iterations is clearly shown in Fig. 16. From Fig. 15 we can see that the control digital voltages Vcc_1 and Vcc_6 converge to positive values. The reactance values of x_1 and x_6 are tuned to high capacitance [see (23)]. Others are tuned to be negative which result in low capacitances. Among them, the capacitances x_2 and x_3 are the smallest. This could be clearly explained with a look at the geometry (Fig. 3) of the ESPAR antenna. Because the desired signal is at 0° in the azimuth plane and the interference is at the 90°. The ESPAR antenna, by tuning the reactance values adaptively to the signal environment, exhibits more directive beam in 0° direction while nulls in 90° (see Fig. 16). As the load capacitance values are varied, the parasitic monopoles' resonant frequencies change, thus the electrical lengths of the elements vary. The parasitic elements surrounding the active central element act like the directors or reflectors respectively as in a Yagi–Uda antenna to maximally receive the desired signals. Therefore the first element (♯1 in Fig. 3) is tuned to be a director while the second (♯2) and third (♯3) elements are adjusted to be reflectors to reject the interference. For DBF array antennas, beamforming is achieved by summing the (phase and amplitude) weighted signals. MBF is based on the same mechanism by move the weighting up to the RF front end.

The constellations of the received baseband BPSK signals before and after the iterations are shown in Fig. 17(a) and (b), respectively. At the beginning of the iteration, the BPSK signal constellation is distorted as shown in Fig. 17(a). After the convergence of the algorithm, the correct constellation is shown in Fig. 17(b). The CCC reaches 0.98. The output SINR is 13 dB.

Next, the DOA of the interference signal is changed to 225°. The averaged output SINR for ten tests is 14.5 dB with a 5.4 dB standard deviation. The averaged beam pattern, obtained with 1,000-bit data samples ($P = 1{,}000$) is plotted in Fig. 18. A 24-dB null is formed toward the interference direction. However, when we moved the interferer to 315°, which is only 45° away from the desired signal, the performance degrades. The beam pattern is plotted in Fig. 19. The averaged output SINR is 6 dB with 1.4-dB standard deviation. This is because the interference is close to the desired signal. Their spatial correlation coefficient reaches 0.7.

We also have tested the beamforming ability when there are two interferences. The SIR is kept at 0 dB. The SNR is still 20 dB. The simulation results with the same condition are shown in Fig. 8 and output SINR data is produced in Table III. The averaged output SINRs over 10 experiments with $P = 50$ are listed in Table IV. For $P = 1{,}000$, measured beam patterns for two cases (case I-desired signal is at 0° and interferers are at 90° and 270°; case II-desired signal is at 0° and interferers are at 225° and 270°) are shown in Figs. 20 and 21, respectively.

The experiment output SINRs and the null levels (see Table IV) agree with the simulation results (see Tables II and III). Nulls could still be formed even there are two interferences; but when the interferer is close to the desired signal (see Fig. 19), or the two interferers are separated with a large angle (see Fig. 20), the null forming performance degrades, which leads to a lower output SINR. The performance is better when one interferer is at 90° or at 225° as shown in Figs. 16 and 18; or when the two interferers are close as in Fig. 21.

There are a few reasons that limit the beamforming performance of the ESPAR antenna. The first one is the range of the reactance values. As we have mentioned in Section V-C, when the desired reactance values exceed the practical reactance range, the value has to be assigned the maximum or the minimum values. It is foreseeable that broadening the reactance ranges brings an improvement in the performance, but there is a practical limitation in this case.

The second reason is that the ESPAR has only seven elements (six parasitic elements). It is reasonable to increase the number of the parasitic elements. As more parasitic elements could function as directors (as in a Yagi–Uda antenna), sharper beam patterns could be formed.

Finally, the ESPAR antenna does not form sharp beams/nulls when there are more than one interferer. This is because the algorithm does not explore the spatial information or the channel information. The beamforming is done only based on the maximization of the CCC through the iteration. The performance could be further enhanced by exploring more channel information, for example, the DOA information by the modified MUSIC algorithm [10], [11].

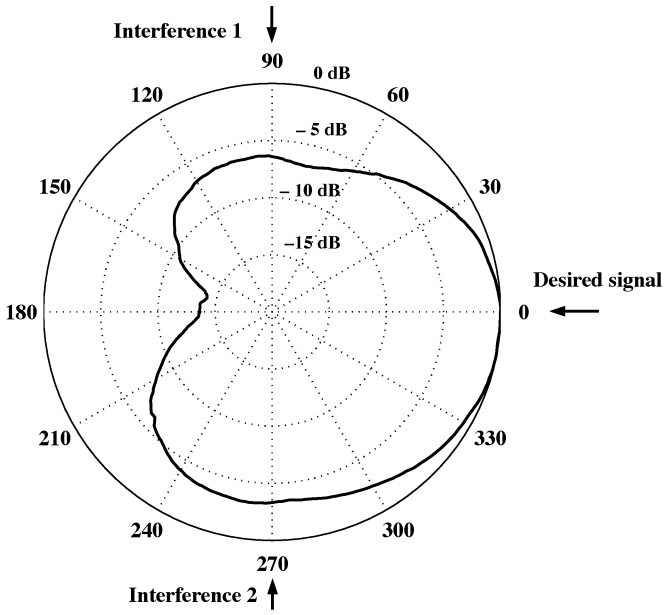

Fig. 20. Measured azimuthal beam pattern ($P = 1000$). DOAs of the desired signal and two interference signals are 0°, 90° and 270°, respectively.

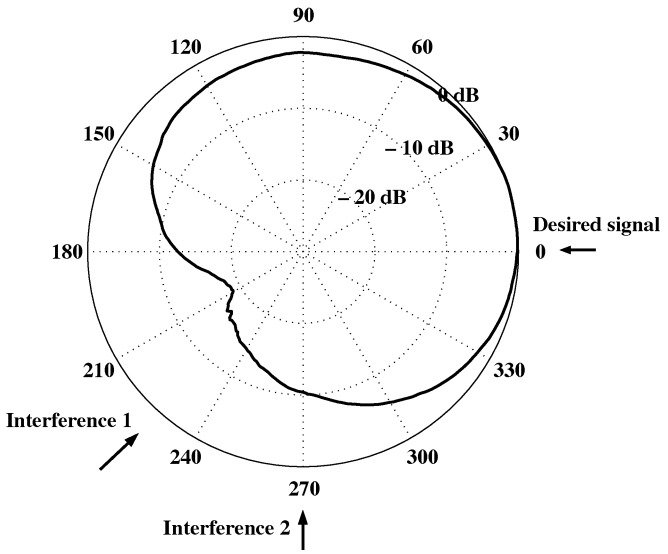

Fig. 21. Measured azimuthal beam pattern ($P = 1000$). DOAs of the desired signal and two interference signals are 0°, 225° and 270°, respectively.

The beauty of the algorithm is that when we increase the number of the elements, the total training signals remains unchanged. Because only two measurements of the objective function are required to calculate the gradient at each iteration stage, which is not dependent on the number of parameters (number of parasitic elements). Therefore, the total number of training bits $(P \times 2 \times N)$ remains unchanged. This is the most attractive feature of the proposed algorithm. With more parameters to optimize, the advantage of SPSA beamforming algorithm over other algorithms becomes more obvious.

VII. Conclusion

In this paper, an economical solution to the deployment of smart antennas at WLAN mobile terminals has been presented. We first described the design of the ESPAR antenna. A fast beamforming algorithm based on SPSA was proposed. The simulation and experiments were carried out to justify the algorithm. In a moderate noisy environment (SNR = 20–30 dB, SIR = 0 dB), the algorithm converges within 5000 data bits, achieving an output SINR of around 10 dB. Thus, a sound communication link (BER ≤ 0.001) could be established quickly.

The results showed that the proposed method is good at interference suppression. Nulls could be formed at the interferers' directions within a few iterations. This proves that ESPAR antennas are suitable for ad hoc networkings or WLAN applications, where the performance is mainly influenced by the interferences from the neighboring mobile terminals (laptops, personal digital assistants, etc.).

In case the SNR drops to a low level (SNR < 10 dB), the performance with respect to the output SINR deteriorates. This indicates that MCCC based algorithm with training signals is not sufficient for noise suppression. Unlike the minimum variance beamforming algorithm [23], the algorithm does not limit the total output power, while it only maximizes the CCC between the reference signals and the training signals. To keep a sound communication, power control algorithms should be employed at the transmitter to keep the SNR at a certain level.

Compared to the DBF antenna arrays and MBF antennas, the ESPAR antennas feature low-power consumption, low cost and ease of fabrication. The smart antenna is efficient because the beamforming is realized at the analog front end instead of at the digital baseband. The proposed fast beamforming algorithm makes the ESPAR antenna a suitable candidate for the mass implementation of the smart antennas, especially at the battery operated wireless mobile terminals.

Appendix

The mutual admittances are obtained with NEC as follows:

$$
\begin{aligned}
y_{00} &= 0.000\,233\,44 - i0.006\,691\,8;\\
y_{10} &= -0.000\,181\,6 + i0.002\,424\,69;\\
y_{11} &= 0.003\,006\,76 - i0.004\,417\,6;\\
y_{21} &= 0.000\,974\,27 + i0.002\,999\,86;\\
y_{31} &= -0.000\,306\,6 - i0.000\,306\,7;\\
y_{41} &= -0.000\,097\,3 - i0.000\,135\,3.
\end{aligned}
$$

Acknowledgment

The authors would like to express their sincere gratitude to Dr. B. Komiyama for his continuous encouragement and helpful suggestions in this work. The authors would also like to express their appreciation to Dr. Q. Han, Dr. T. Hunziker, K. Iigusa, M. Hashiguchi, and E. Taillefer for their helpful discussions.

References

[1] J. C. Liberti and T. S. Rappaport, *Smart Antennas for Wireless Communications: IS-95 and Third Generation CDMA Applications*. Englewood Cliffs, NJ: Prentice-Hall, 1999, pp. 285–305.

[2] G. V. Tsoulos, "Smart antennas for mobile communication systems: Benefits and challenges," *Electron. Comm. Eng. J.*, vol. 11, no. 2, pp. 84–94, Apr. 1999.

[3] R. Ramanathan and J. Redi, "A brief overview of ad hoc networks: Challenges and directions," *IEEE Commun. Mag.*, vol. 40, pp. 20–22, May 2002.

[4] L. C. Godara, "Application of antenna arrays to mobile communications, part II: Beam-forming and direction-of-arrival considerations," *Proc. IEEE*, vol. 85, pp. 1195–1245, Aug. 1997.
[5] T. Ohira, "Adaptive array antenna beamforming architectures as viewed by a microwave circuit designer," in *Proc. IEEE Asia-Pacific Microwave Conf.*, Sydney, Australia, Dec. 2000, pp. 828–833.
[6] T. Ohira, Y. Suzuki, H. Ogawa, and K. Kamitsuna, "Megalithic microwave signal processing for phased-array beamforming and steering," *IEEE Trans. Microwave Theory Tech.*, vol. 45, pp. 2324–2332, Dec. 1997.
[7] R. F. Harrington, "Reactively controlled directive arrays," *IEEE Trans. Antennas Propagat.*, vol. AP-26, pp. 390–395, May 1978.
[8] R. Schlub, J. Lu, and T. Ohira, "Seven element ground skirt monopole ESPAR antenna design using a genetic algorithm and the finite element method," *IEEE Trans. Antennas Propagat*, vol. 51, pp. 3033–3039, Nov. 2003.
[9] T. Ohira and K. Gyoda, "Hand-held microwave direction-of-arrival finder based on varactor-tuned analog aerial beamforming," in *Proc. IEEE Asia–Pacific Microwave Conf.*, Taipei, Taiwan, R.O.C., Dec. 2001, pp. 585–588.
[10] C. Sun and N. C. Karmakar, "A DOA estimation technique based on a single-port smart antenna for position location services," in *Proc. Asia–Pacific Microwave Conf.*, Kyoto, Japan, Nov. 2002, pp. 196–199.
[11] C. Plapous, J. Cheng, E. Taillefer, A. Hirata, and T. Ohira, "Reactance domain MUSIC algorithm for electronically steerable parasitic array radiator," IEEE Trans. Antennas Propagat, vol. 52, 2004, to be published.
[12] E. Taillefer, C. Plapous, J. Cheng, K. Iigusa, and T. Ohira, "Reactance-domain MUSIC for ESPAR antennas (experiment)," in *Proc. Wireless Communications Network Conf., WCNC2003*, Mar. 2003, pp. 98–102.
[13] A. Hirata, H. Yamada, and T. Ohira, "Reactance-domain MUSIC DOA estimation using calibrated equivalent weight matrix of ESPAR antenna," in *Proc. IEEE Antennas and Propagation Soc. Int. Symp.*, June 2003, pp. 252–255.
[14] A. Hirata, T. Aono, H. Yamada, and T. Ohira, "Reactance-domain SSP MUSIC for an ESPAR antenna to estimate the DOAs of coherent waves," in *Proc. Int. Symp. Wireless Personal Multimedia Communications*, Yokosuka, Japan, Oct. 2003, pp. 242–246.
[15] J. Cheng, Y. Kamiya, and T. Ohira, "Adaptive beamforming of ESPAR antenna using sequential perturbation," in *Proc. IEEE MTT-S Int. Microwave Symp. Dig.*, vol. 1, May 2001, pp. 133–136.
[16] B. Shishkov and T. Ohira, "Adaptive beamforming of ESPAR antenna based on stochastic approximation theory," in *Proc. IEEE Asia–Pacific Microwave Conf.*, vol. 2, Dec. 2001, pp. 597–600.
[17] C. Sun and N. C. Karmakar, "Adaptive beamforming of ESPAR antenna based on simultaneous perturbation stochastic approximation theory," in *Proc. Asia–Pacific Microwave Conf.*, Kyoto, Japan, Nov. 2002, pp. 192–195.
[18] T. Ohira, "Blind aerial beamforming based on a higher-order maximum moment criterion (part I: Theory)," in *Proc. Asia–Pacific Microwave Conf.*, Kyoto, Japan, Nov. 2002, pp. 181–184.
[19] J. Cheng, K. Iigusa, M. Hashiguchi, and T. Ohira, "Blind aerial beamforming based on a higher-order maximum moment criterion (part II: Experiments)," in *Proc. Asia–Pacific Microwave Conf.*, Kyoto, Japan, Nov. 2002, pp. 185–188.
[20] A. Hirata and T. Ohira, "Spotted null forming of electronically steerable parasitic array radiator antennas in indoor multipath propagation," in *Proc. Asia–Pacific Microwave Conf.*, Kyoto, Japan, Nov. 2002, pp. 189–191.
[21] C. A. Balanis, *Antenna Theory: Analysis and Design*, 2nd ed. New York: Wiley, 1997, pp. 127–257.
[22] B. Widrow, P. E. Mantey, L. J. Griffiths, and B. B. Goode, "Adaptive antenna systems," *IEEE Trans. Antennas Propagat.*, vol. AP-55, pp. 2143–2159, Dec. 1967.
[23] D. H. Johnson and D. E. Dudgeon, *Array Signal Processing: Concepts and Techniques*. Englewood Cliffs, NJ: Prentice-Hall, 1993, pp. 111–365.
[24] S. Haykin, *Adaptive Filter Theory*. Upper Saddle River, NJ: Prentice-Hall, 2002, pp. 231–319.
[25] T. Moon and W. Stirling, *Mathematical Methods and Algorithms for Signal Processing*. Upper Saddle River, NJ: Prentice-Hall, 2001, pp. 637–643.
[26] H. J. Kushner and G. G. Yin, *Stochastic Approximation Algorithms and Applications*. New York: Springer, 1997, pp. 1–25.
[27] J. C. Spall, "Implementation of the simultaneous perturbation algorithm for stochastic optimization," *IEEE Trans. Aerosp. Electron. Syst.*, vol. 34, pp. 817–823, July 1998.
[28] [Online]. Available: http://www.chipdocs.com
[29] M. Wennstrom, "Smart antenna implementation issues for wireless communications," Ph.D. dissertation, Uppsala Univ., Sweden, Oct. 1999, pp. 29–59.
[30] P. Howard, C. M. Simmonds, P. Darwood, M. A. Beach, R. Arnott, F. Cesbron, and M. Newman, "Adaptive antenna performance in mobile systems,", Tech. Rep. ERA 98-0797, Oct. 1998 pp. 330-335.
[31] P. E. Mogensen, K. I. Pedersen, P. L. Espensen, B. Fleury, F. Frederiksen, K. Olesen, and S. L. Larsen, "Preliminary measurement results from an adaptive antenna array testbed for GSM/UMTS," in *Proc. IEEE 47th Vehicular Technology Conf.*, vol. 3, May 1997, pp. 1592–1596.
[32] T. Ohgane, Y. Ogawa, and K. Itoh, "A study on a channel allocation scheme with an adaptive array in SDMA," in *Proc. IEEE VTC'97*, vol. 2, May 1997, pp. 725–729.
[33] C. Sun and N. C. Karmakar, "Null-forming SDMA scheme based on channel responses correlation coefficient," in *Proc. IEEE Antennas and Propagation Soc. Int. Symp.*, OH, June 2003, pp. 85–88.
[34] J. Cheng, M. Hashiguchi, K. Iigusa, and T. Ohira, "Electronically steerable parasitic array radiator antenna for omni- and sector-pattern forming applications to wireless ad hoc networks," in *Proc. Inst. Elect. Eng. Antennas and Propagation*, vol. 150, Aug. 2003, pp. 203–208.

Chen Sun (S'02) received the B.Eng. degree (first honors) in electronics from Northwestern Polytechnical University, Xi'an, China, in 2000 and is currently working toward the Ph.D. degree at Nanyang Technological University, Singapore.

From November 2002 to March 2003, he was a Student Intern with ATR Adaptive Communications Research Laboratories, Kyoto, Japan, working on personal wireless links for wireless ad hoc networks. His research interests include array signal processing, diversity combining techniques, MIMO communications and array antenna design.

Akifumi Hirata (M'03) received the B.E. and M.E. degrees in electrical engineering from Osaka Prefecture University, Osaka, Japan, in 1994 and 1996, respectively.

In 1996, he joined the SANYO Electric Company, Ltd., Gifu, Japan, where he was engaged in research on telecommunication systems and developed software of Personal Handy phone System (PHS) base stations. Since 2001, he has been engaged in research on wireless ad hoc networks and microwave analog adaptive antennas for mobile user terminals at Adaptive Communications Research Laboratories, Advanced Telecommunications Research Institute International (ATR), Kyoto, Japan.

Mr. Hirata is a recipient of the 2002 Institute of Electrical, Information and Communication Engineers (IEICE) of Japan Young Engineer Award.

Takashi Ohira (S'79–M'83–SM'99–F'04) received the B.E. and D.E. degrees in communication engineering from Osaka University, Osaka, Japan, in 1978 and 1983, respectively.

In 1983, he joined NTT Electrical Communication Laboratories, Yokosuka, Japan, where he was engaged in research on monolithic integration of microwave semiconductor devices and circuits. He developed GaAs MMIC transponder modules and microwave beamforming networks aboard Japanese domestic multibeam communication satellites, Engineering Test Satellite VI (ETS-VI) and ETS-VIII, at NTT Wireless Systems Laboratories, Yokosuka. Since 1999, he has been engaged in research on wireless ad hoc networks and microwave analog adaptive antennas in consumer electronic devices at Adaptive Communications Research Laboratories, Advanced Telecommunications Research Institute International (ATR), Kyoto, Japan. Concurrently, he was a Consulting Engineer for the National Astronautical Space Development Agency (NASDA) ETS-VIII Project in 1999, and an Invited Lecturer at Osaka University in 2000 to 2001. He coauthored *Monolithic Microwave Integrated Circuits* (Tokyo, Japan: IEICE, 1997).

Dr. Ohira was awarded the 1986 Institute of Electrical, Information and Communication Engineers (IEICE) of Japan Shinohara Prize and the 1998 Japan Microwave Prize. He serves as IEEE MTT-S Japan Chapter Vice-Chairperson.

Nemai C. Karmakar (S'91–M'92–SM'99) received the M.Sc. degree in electrical engineering from the University of Saskatchewan, SK, Canada, in 1991 and the Ph.D. degree from the University of Queensland, Brisbane, Australia, in 1999. His Ph.D. dissertation concerned the area of switched beam and phased array antennas for mobile satellite communications, and was one of the most significant findings at The University of Queensland in 1998 and published in national media such as ABC Radio and *Canberra Times*.

Between 1989 and 1990, he was an Assistant Engineer with the Electronics Institute, Atomic Energy Research Establishment, Dhaka, Bangladesh. In August 1990, he was a Research Assistant at the Communications Research Group, University of Saskatchewan. From 1992 to 1995, he was a Microwave Design Engineer at Mitec Ltd., Brisbane, Australia, where he contributed to the development of land mobile satellite antennas for the Australian Mobilesat. From 1995 to 1996, he taught final year courses on microwaves and antenna technologies at Queensland University of Technology, Brisbane, Australia. From September 1998 to March 1999, he worked as a Research Engineer within the Radar Laboratory, Nanyang Technological University, Singapore. Since March 1999, he has been an Assistant Professor and Graduate Advisor in the Division of Communication Engineering, School of Electrical and Electronic Engineering, Nanyang Technological University, Singapore. In August 2004, he is scheduled to join the Department of Electrical and Computer Systems Engineering, Monash University, Victoria, Australia, as a Senior Lecturer. He has published more than 120 refereed journal and conference papers, and six book chapters. His research interests cover areas such as smart antennas, EBG assisted RF devices, planar phased array antennas, broadband microstrip antennas and arrays, beam-forming networks, near-field/far-field antenna measurements, microwave device modeling, monostatic and bistatic radars. His biography has been included in Marquis *Who's Who in Science and Technology 2002–2003* edition as a pioneer in planar phased arrays.